Disrupted cholesterol metabolism promotes age-related photoreceptor neurodegeneration[S]

Norimitsu Ban,* Tae Jun Lee,* Abdoulaye Sene,* Zhenyu Dong,* Andrea Santeford,* Jonathan B. Lin,*,† Daniel S. Ory,§ and Rajendra S. Apte[1],*,†,**

Departments of Ophthalmology and Visual Sciences* and Medicine and Developmental Biology,** Neuroscience Graduate Program, Division of Biology and Biomedical Sciences,† and Diabetic Cardiovascular Disease Center,§ Washington University School of Medicine in St. Louis, St. Louis, MO 63110

Abstract Photoreceptors have high intrinsic metabolic demand and are exquisitely sensitive to metabolic perturbation. In addition, they shed a large portion of their outer segment lipid membranes in a circadian manner, increasing the metabolic burden on the outer retina associated with the resynthesis of cell membranes and disposal of the cellular cargo. Here, we demonstrate that deletion of both ABCA1 and ABCG1 in rod photoreceptors leads to age-related accumulation of cholesterol metabolites in the outer retina, photoreceptor dysfunction, degeneration of rod outer segments, and ultimately blindness. A high-fat diet significantly accelerates rod neurodegeneration and vision loss, further highlighting the role of lipid homeostasis in regulating photoreceptor neurodegeneration and vision.—Ban, N., T. J. Lee, A. Sene, Z. Dong, A. Santeford, J. B. Lin, D. S. Ory, and R. S. Apte. **Disrupted cholesterol metabolism promotes age-related photoreceptor neurodegeneration. *J. Lipid Res.* 2018.** 59: **1414–1423.**

Supplementary key words ATP binding cassette transporter G1 • cholesterol/dietary • cholesterol/efflux • eye/retina • neurons • aging

Metabolic neurodegeneration is a central feature of diverse age-related pathologies such as Alzheimer's disease (1) and retinal degeneration (2). The neurosensory retina, an extension of the CNS, is a complex neurovascular tissue whose primary function is to process light and color perceived by photoreceptor neurons and transmit this information to the visual cortex for further processing in order to generate a precise visual image. In the neurosensory retina, photoreceptor degeneration causes blindness in diseases such as retinitis pigmentosa (3) and age-related macular degeneration (AMD) (4).

The retina is also the most metabolically active tissue in the body (5, 6) and is exquisitely sensitive to metabolic flux (7). A significant portion of this metabolic demand is related to the circadian shedding of about ten percent of photoreceptor lipid bilayer membranes (7, 8). Photoreceptor outer segments once shed have to be regenerated, placing a very high biochemical burden on these cells. In addition, the lipid-rich shed outer segments have to be processed by the retinal pigment epithelium (RPE) underneath the neurosensory retina (9).

These cholesterol-containing lipids are then packaged onto carrier lipoproteins for transport from the eye to the bloodstream using a well-characterized process called reverse cholesterol transport or cholesterol efflux (7, 10). ABCA1 and ABCG1 play a central role in coordinating reverse cholesterol transport by packaging cholesterol and other lipids onto apolipoprotein carriers, such as ApoA1 and HDL, for transport through the blood stream to the liver (10, 11). For these reasons, we hypothesized that maintaining physiologic cholesterol homeostasis by ABCA1 and ABCG1 would play a key role in photoreceptor function and survival. In the retina, there are two types of photoreceptors: rods responsible for dim vision and cones responsible for color and daytime vision. Although ABCA1 and ABCG1 have been reported to be expressed in the

This work was supported by National Institutes of Health Grants R01 EY019287 (R.S.A.) and P30 EY02687 (Vision Core Grant), the International Retinal Research Foundation (N.B.), the Starr Foundation (R.S.A.); the Carl Marshall and Mildred Almen Reeves Foundation (R.S.A.); the Bill and Emily Kuzma Family Gift for Retinal Research (R.S.A.), Research to Prevent Blindness Physician-Scientist and Nelson Trust Awards (R.S.A.), the Jeffrey Fort Innovation Fund (R.S.A.); the Glenn Foundation for Medical Research, and the Thome Memorial Foundation (R.S.A.). Additional support was provided by an unrestricted Research to Prevent Blindness Grant to the Department of Ophthalmology and Visual Sciences of Washington University School of Medicine. J.B.L. was supported by the Washington University in St. Louis Medical Scientist Training Program (National Institutes of Health Grant T32 GM07200), the Washington University in St. Louis Institute of Clinical and Translational Sciences (National Institutes of Health Grants UL1 TR002345 and TL1 TR002344), and the VitreoRetinal Surgery Foundation. The content is solely the responsibility of the authors and does not necessarily represent the official views of the National Institutes of Health. The authors declare that they have no conflict of interest.

Manuscript received 16 February 2018 and in revised form 12 June 2018.

Published, JLR Papers in Press, June 26, 2018
DOI https://doi.org/10.1194/jlr.M084442

Abbreviations: AMD, age-related macular degeneration; CE, cholesteryl ester; ERG, electroretinography; HC, hydroxycholesterol; HFD, high-fat diet; RPE, retinal pigment epithelium.

[1] To whom correspondence should be addressed.
e-mail: apte@wustl.edu

[S] The online version of this article (available at http://www.jlr.org) contains a supplement.

retina, including in photoreceptors (12, 13), their function in photoreceptor physiology is largely unknown. In order to assess the functions of ABCA1 and ABCG1 in photoreceptors, we generated mice lacking both *Abca1* and *Abcg1* specifically from either rods (14, 15) or cones (15, 16). Retinas were structurally evaluated by biomicroscopy, histology, and electron microscopy at 3–18 months of age. In addition, retinal function and vision were evaluated by electrophysiology.

MATERIALS AND METHODS

Animals

All animal experiments were conducted in accordance with Washington University in St. Louis School of Medicine Animal Care and Use guidelines after approval by the Animal Studies Committee. All mice were housed in a temperature-controlled room under a 12 h light/dark cycle, with free access to food and water. All mouse species used in the experiments are summarized in **Table 1**. *Abca1/g*$^{F/F}$ mice were previously characterized (17, 18) and were purchased commercially (Jackson Laboratory, Bar Harbor, ME). To generate mice lacking both *Abca1* and *Abcg1* specifically from rod photoreceptors, we crossed *Abca1/g1*$^{F/F}$ mice with mice carrying one copy of the rhodopsin-iCre75 (Rhod-iCre) transgene, which were provided by Dr. Ching-Kang Jason Chen and have been previously characterized (14, 15). To generate mice lacking both *Abca1* and *Abcg1* specifically from cone photoreceptors, we crossed *Abca1/g1*$^{F/F}$ mice with mice carrying one copy of the human red/green pigment-Cre (HRGP-Cre) transgene, which were provided by Dr. Yun Le and have been previously characterized (15, 16, 19). We confirmed that these mice did not carry the *Crb1* gene *rd8* mutation (20) (data not shown). For high-fat diet (HFD) feeding experiments, only male *Abca1/g1*$^{F/F}$ and *Abca1/g1*$^{-rod/-rod}$ mice were used. We used an adjusted-calorie diet (42% from fat, 43% kcal from carbohydrate, and 15% kcal from protein; TD.88137; ENVIGO, Indianapolis, IN) (21) as a HFD, starting from 6 weeks old to the target age of analysis. We used Purina 4043 chow (13% kcal from fat, 62% kcal from carbohydrate, 25% kcal from protein) as the normal diet (21).

Isolation of rod or cone photoreceptors from the retina

To isolate rod or cone photoreceptors from the retina, we used the Papain Dissociation System (Worthington Biochemical Corporation, Lakewood, NJ) following a previously described modified protocol (22), followed by EasySep Mouse PE or FITC positive selection kit (Stem Cell Technologies, Vancouver, Canada), respectively, following the manufacturer's protocol. We used 1 μg/ml of PE-conjugated anti-CD73 antibodies (Miltenyi Biotec, Bergisch Gladbach, Germany) (15) for rod photoreceptors and 5 μg/ml of fluorescein peanut agglutinin (Vector Laboratories, Burlingame, CA) (23) for cone photoreceptors, respectively.

TABLE 1. Mouse abbreviations

Abbreviations	Genotype
Abca1/g$^{F/F}$	*Abca1*$^{flox/flox}$ and *Abcg1*$^{flox/flox}$ Cre-negative
Abca1/g1$^{-rod/-rod}$	*Abca1*$^{flox/flox}$ and *Abcg1*$^{flox/flox}$ Rhod-iCre positive
Abca1/g1$^{-cone/-cone}$	*Abca1*$^{flox/flox}$ and *Abcg1*$^{flox/flox}$ HRGP-Cre positive
Abca1/g1$^{+rod/-rod}$	*Abca1*$^{-/flox}$ and *Abcg1*$^{-/flox}$ Rhod-iCre positive
Abca1/g$^{-F/-F}$ *Rhod-iCre*	*Abca1*$^{-/-}$ and *Abcg1*$^{-/-}$ Rhod-iCre positive

RNA isolation and quantitative PCR

Total RNA was extracted using an RNeasy Micro Plus kit (Qiagen, Hilden, Germany) according to the manufacturer's instructions. To synthesize cDNA, total RNA was added to the high-capacity cDNA reverse transcription kits (Thermo Fisher Scientific, Waltham, MA) and reverse-transcribed according to manufacturer's instructions. Quantitative (q)PCR was performed in duplicate using the StepOnePlus real-time PCR system (Thermo Fisher Scientific) using TaqMan real-time PCR assays (Thermo Fisher Scientific), and the mRNA was quantified using the ΔΔCT method with *Gapdh* or *Actb* as the internal control.

Electroretinography

Electroretinography (ERG) was performed as previously described (21). A UTAS BigShot system (LKC Technologies, Inc., Gaithersburg, MD) was used. Mice were dark adapted overnight. Under red light illumination, mice were anesthetized with an intraperitoneal injection of 86.9 mg/kg ketamine and 13.4 mg/kg xylazine. Pupils were dilated with 1% atropine sulfate eye drops (Bausch and Lomb, Rochester, NY). Body temperature was maintained at 37°C with a heating pad. Contact lens electrodes were placed bilaterally with appropriate reference and ground electrodes. The stimuli consisted of a full-field white light flash (10 μs) in darkness or in the presence of dim [30.0 candela (cd)/m^2] background illumination after 10 min adaptation time. Raw data were processed using MATLAB software (MathWorks, Natick, MA). The amplitude of the a-wave was measured from the average pretrial baseline to the most negative point of the average trace, and the b-wave amplitude was measured from that point to the highest positive point.

Retinal imaging

We performed digital color fundus photography and optical coherence tomography, as previously described (15, 24), using the Micron III animal fundus camera equipped with 830 nm optical coherence tomography (Phoenix Research Labs, Pleasanton, CA). Prior to fundus imaging and optical coherence tomography, we anesthetized mice with an intraperitoneal injection of 86.9 mg/kg ketamine and 13.4 mg/kg xylazine and administered 1.0% tropicamide eye drops (Bausch and Lomb) to dilate the pupils.

Transmission electron microscopy

We performed transmission electron microscopy analysis as previously described (15). For ultrastructural analyses, samples were fixed in 2% paraformaldehyde/2.5% glutaraldehyde (Polysciences Inc., Warrington, PA) in 100 mM sodium cacodylate buffer (pH 7.2) for 2 h at room temperature and then overnight at 4°C. Samples were washed in sodium cacodylate buffer at room temperature and postfixed in 1% osmium tetroxide (Polysciences Inc.) for 1 h. Samples were then rinsed extensively in dH_2O prior to en bloc staining with 1% aqueous uranyl acetate (Ted Pella Inc., Redding, CA) for 1 h. Following several rinses in dH_2O, samples were dehydrated in a graded series of ethanol and embedded in Eponate 12 resin (Ted Pella Inc.). Sections of 95 nm were cut with a Leica Ultracut UCT ultramicrotome (Leica Microsystems Inc., Bannockburn, IL), stained with uranyl acetate and lead citrate, and viewed on a JEOL 1200 EX transmission electron microscope (JEOL USA Inc., Peabody, MA) equipped with an AMT 8 megapixel digital camera and AMT Image Capture Engine V602 software (Advanced Microscopy Techniques, Woburn, MA).

Analysis of total cholesterol in the neurosensory retina

We used Amplex Red cholesterol assay kits (Thermo Fisher Scientific) to measure total cholesterol in the neurosensory retina

following the manufacturer's protocol. Each neurosensory retina was homogenized with RIPA buffer (Thermo Fisher Scientific). Cholesterol concentrations were normalized to wet weights of the neurosensory retina (milligrams).

Analyses of HDL, LDL/VLDL, and ApoA-1 in serum

We collected blood samples from facial veins after overnight fasting. Blood samples were centrifuged at 800 *g* for 15 min, and then serum samples were collected. HDL and LDL/VLDL in serum were measured using HDL and LDL/VLDL quantitation kits (Sigma, St. Louis, MO) following the manufacturer's protocol. ApoA-1 in serum was measured using an ApoA1 ELISA kit (LifeSpan BioSciences, Seattle, WA) following the manufacturer's protocol.

Analyses of oxysterols, free cholesterol, and cholesteryl esters in RPE complex

To prepare RPE/choroid/sclera samples, we dissected the eyeballs to remove the anterior parts, including cornea, lens, and iris. After removing neurosensory retina, RPE/choroid/sclera samples were flash-frozen with liquid nitrogen and then stored at −80°C until the analyses. This RPE/choroid/sclera sample was named the RPE complex.

Each RPE complex was homogenized with 50-fold excess volume of PBS buffer using Omni Bead Ruptor 24 (Omni International Inc., Kennesaw, GA). All of the analytes listed above in 50 μl of the mouse retina homogenate were extracted with 200 μl of methanol. Prior to the extraction, triol-d7 (2 ng), 7-ketocholesterol-d7 (2 ng), 24-hydroxycholesterol (HC)-d7 (2 ng), 27-HC-d5 (2 ng), 4β-HC-d7 (2 ng), cholesteryl esters (CEs) (18:2)-d7 (200 ng), and cholesterol-d7 (1 μg) were added as the internal standards to the homogenate samples. All oxysterols and cholesterol, as well as their deuterated standards, were derivatized with *N,N*-dimethylglycine to increase the MS sensitivity. Cholesteryl esters were not derivatized for the MS analyses.

The analysis of oxysterols and free cholesterol was performed with a Shimadzu 20AD HPLC system and a Shimadzu SIL 20AC autosampler coupled to a triple quadrupole mass spectrometer (API-6500Qtrap+; Thermo Fisher Scientific) operated in MRM mode. The positive ion ESI mode was used for detection of the *N,N*-dimethylglycine-derivatized oxysterols and free cholesterol. An Agilent Ecrips XDB-C18 HPLC column (3.0 × 100 mm, 3.5 μm) was used for separation of all oxysterols. Mobile phase (a) 1% formic acid in water and mobile phase (b) 1% formic acid in 1:1 methanol/acetonitrile were programmed from 60% (b) to 99% in 4 min at a flow rate of 0.9 ml/min. All samples were injected in duplicate for data averaging. Data processing was conducted with Analyst 1.6.3 (Thermo Fisher Scientific).

The analysis of two cholesteryl esters [CE(16:0) and CE(18:0)] was performed with a Shimadzu 20AD HPLC system, a LeapPAL autosampler coupled to a triple quadrupole mass spectrometer (API 4000; Thermo Fisher Scientific) operated with positive ion MRM mode. An Agilent Ecrips XDB-C8 HPLC column (4.6 × 100 mm, 3.5 μm) was used for these cholesteryl esters. The mobile phases, (a) 10 mmol ammonium acetate in 3:7 acetonitrile/water and (b) 10 mmol ammonium acetate in 1:1 methanol/isopropanol, were programmed from 80% (b) to 99% in 4 min and held for 2 min at a flow rate of 1.2 ml/min. The data processing was conducted with Analyst 1.5.1 (Thermo Fisher Scientific).

The analysis of the rest of the cholesteryl esters [CE(16:2), CE(18:1), CE(18:2), and CE(20:4)] was performed with a Shimadzu 10AD HPLC system and a Shimadzu SIL 20AC autosampler coupled to a triple quadrupole mass spectrometer (TSQ Quantum Ultra; Thermo Fisher Scientific) operated in MRM mode. A Thermo-Keystone betasil C18 HPLC column (2.0 × 100 mm, 5 μm) was used for the cholesteryl esters. The identical mobile phases [(a) and (b) listed above] were also used with an isocratic condition at 97% (b) for 12 min at a flow rate of 0.4 ml/min. The data processing was conducted with XCalibur (Thermo-Fisher Scientific).

The relative quantification data is reported as peak area ratios of analytes to their internal standards normalized to wet weights (milligrams) of RPE complex.

Statistics

We performed statistical testing with GraphPad Prism (Version 6.0), using the appropriate test for each dataset. We defined statistical significance as a $P < 0.05$. Values are mean ± SE.

RESULTS

Deletion of *Abca1 and Abcg1* in rod photoreceptors increases retinal cholesterol, but does not affect retinal function in young mice

The deletion of both *Abca1* and *Abcg1* in *Abca1/g1*$^{-rod/-rod}$ mouse rod photoreceptors was confirmed by quantitative (q)PCR (supplemental Fig. S1A). Total cholesterol levels were higher in the neurosensory retinas of *Abca1/g1*$^{-rod/-rod}$ mice compared with littermate controls (*Abca1/g1*$^{F/F}$) (supplemental Fig. S1B). However, *Abca1/g1*$^{-rod/-rod}$ retinas were functionally and histopathologically normal at 3 months of age (**Fig. 1A–**C; supplemental Fig. S1C, D). Serum levels of HDL, LDL/VLDL, and ApoA-1 also did not show any differences (supplemental Fig. S1E–G).

Aged *Abca1/g1*$^{-rod/-rod}$ mice demonstrate lipid accumulation underneath the retina with associated rod neurodegeneration and vision loss

Although young *Abca1/g1*$^{-rod/-rod}$ mice did not demonstrate a functional phenotype at 3 months of age, upon analysis at 12 months of age, both scotopic a- and b-waveforms were significantly attenuated in *Abca1/g1*$^{-rod/-rod}$ mouse retinas compared with littermate controls (Fig. 1D, E) and other controls (supplemental Fig. S2A, B), confirming rod photoreceptor dysfunction and vision loss. In contrast, photopic responses, a measure of cone function, were normal in *Abca1/g1*$^{-rod/-rod}$ mouse retinas (Fig. 1F, supplemental Fig. S2C). Although fundus biomicroscopy at 12 months showed no gross abnormalities (Fig. 1G), electron microscopy demonstrated attenuation of normal vesicular structures at the rod inner and outer segment junction (25) in *Abca1/g1*$^{-rod/-rod}$ mouse retinas (Fig. 1H). In addition, photoreceptor degeneration characterized by outer segment dysmorphic changes was identified in *Abca1/g1*$^{-rod/-rod}$ mouse retinas, while littermate controls were normal (Fig. 1I). These structural changes were also associated with accumulation of large lipid droplets within the RPE (Fig. 1J). Further analysis by LC-MS/MS confirmed an increase in the levels of free cholesterol and several cholesterol metabolites underneath the neurosensory retina in the RPE complex (**Fig. 2A**) with no increase in any of the CEs analyzed (Fig. 2B).

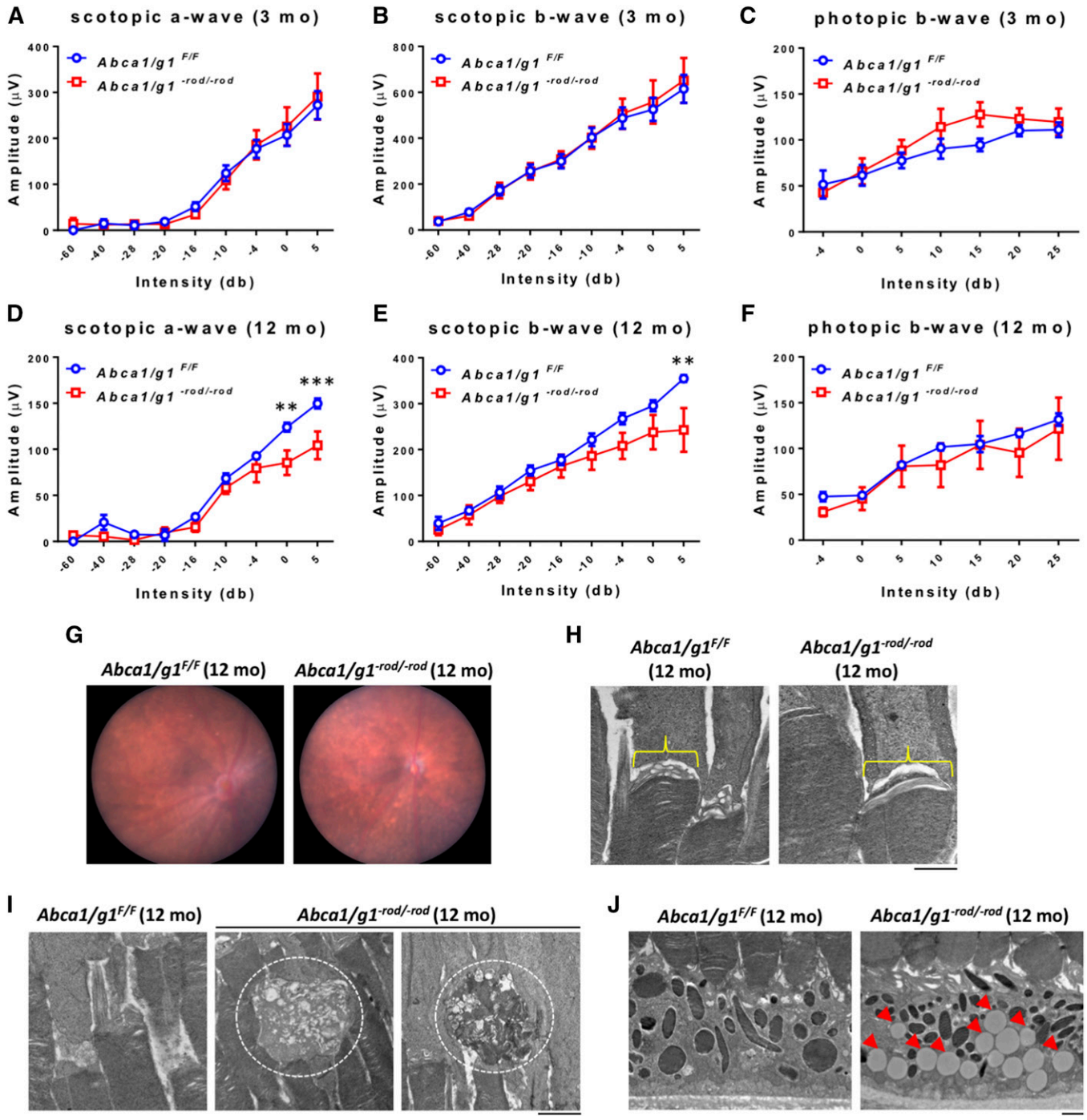

Fig. 1. Aged (12 months) *Abca1/g1*$^{-rod/-rod}$ mouse retinas show decreased scotopic responses and accumulation of lipids. A–C: ERG of 3-month-old *Abca1/g1*$^{F/F}$ and *Abca1/g1*$^{-rod/-rod}$ mice. *Abca1/g1*$^{F/F}$ (blue circles), n = 7; *Abca1/g1*$^{-rod/-rod}$ (red squares), n = 5. A: Scotopic a-wave amplitude. B: Scotopic b-wave amplitude. C: Photopic b-wave amplitude. No significant difference was detected by two-way ANOVA. D–F: ERG of 12-month-old *Abca1/g1*$^{F/F}$ and *Abca1/g1*$^{-rod/-rod}$ mice. *Abca1/g1*$^{F/F}$ (blue squares), n = 5; *Abca1/g1*$^{-rod/-rod}$ (red squares), n = 5. D: Scotopic a-wave amplitude. E: Scotopic b-wave amplitude. F: Photopic b-wave amplitude. $^{**}P < 0.01$ and $^{***}P < 0.001$ by two-way ANOVA with post hoc Bonferroni's multiple comparison test. G: Representative fundus images of 12-month-old *Abca1/g1*$^{F/F}$ and *Abca1/g1*$^{-rod/-rod}$ mouse retinas. H, I: Representative electron microscopy images of 12-month-old *Abca1/g1*$^{F/F}$ and *Abca1/g1*$^{-rod/-rod}$ mouse retinas. Scale bar: 1 μm. H: Attenuation of vesicular structures at the rod inner and outer segment in *Abca1/g1*$^{-rod/-rod}$ mouse retinas. I: Dysmorphic change of outer segments of *Abca1/g1*$^{-rod/-rod}$ mouse retinas (dashed circle). J: Accumulation of large lipid droplets within the RPE (red arrowheads). Values are mean ± SE.

Retinal neurodegeneration increases in severity and affects cone photoreceptors with increasing age

We kept *Abca1/g1*$^{-rod/-rod}$ mice up to 18 months to check to determine whether further aging might affect the neurodegenerative phenotype. At 18 months of age, vision loss was more severe with further degradation of scotopic rod responses on electrophysiology in *Abca1/g1*$^{-rod/-rod}$ mice compared with littermate controls (**Fig. 3A**, B) and other

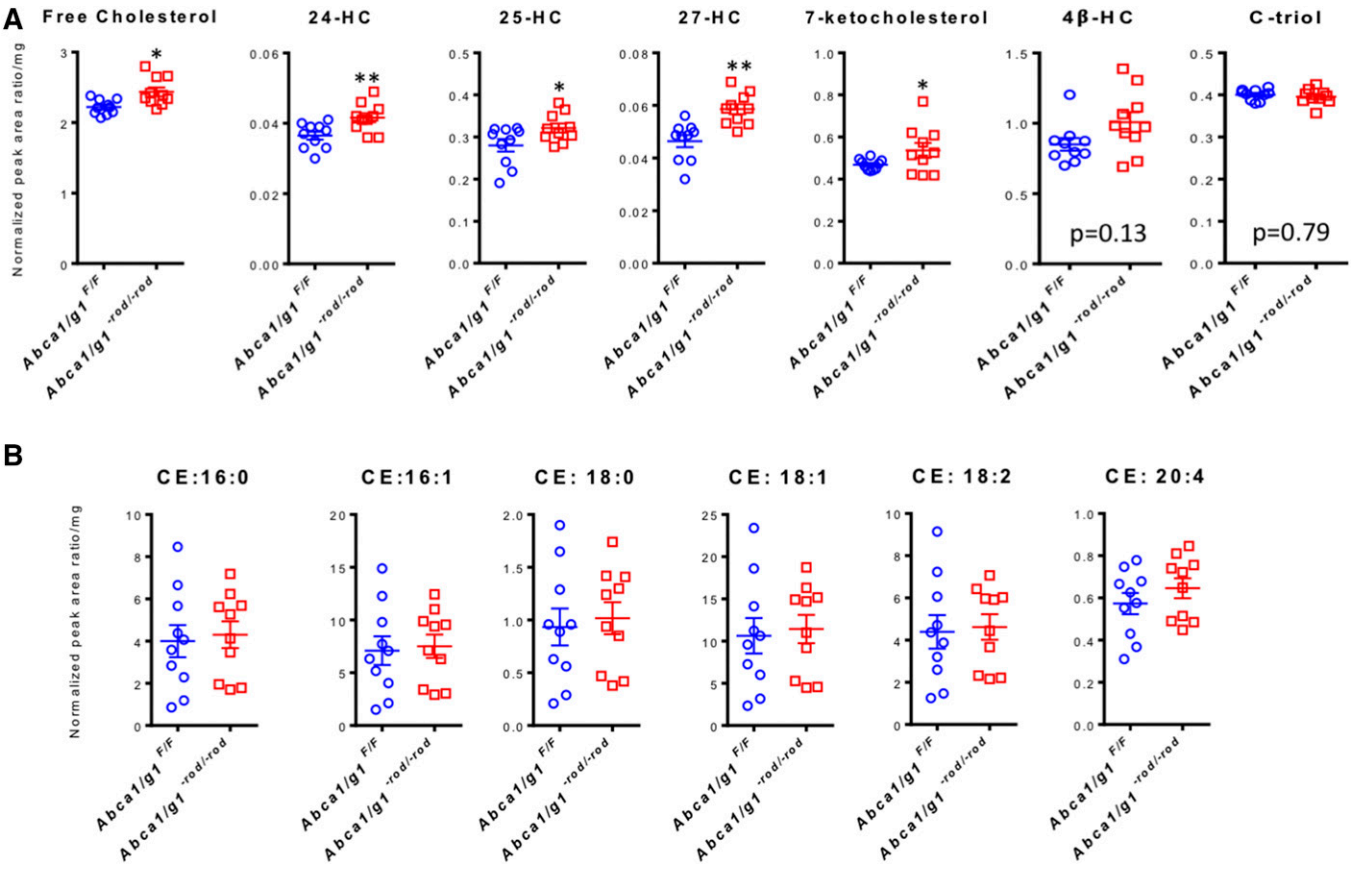

Fig. 2. Lipid analysis of *Abca1/g1*$^{-rod/-rod}$ mouse eyes at 12 months of age demonstrates accumulation of cholesterol metabolites. A: Analyses of free cholesterol, 24-HC, 25-HC, 27-HC, and 7-ketocholesterol underneath the neurosensory retina in the RPE/choroid complex at 12 months of age (normalized peak area ratio per milligram wet tissue weight); n = 10 for each group. *$P < 0.05$ and **$P < 0.01$ by two-tailed unpaired *t*-test. B: Analyses of CEs underneath the neurosensory retina in the RPE/choroid complex at 12 months of age (normalized peak area ratio per milligram wet tissue weight); n = 10 for each group. No significant difference was detected by two-tailed unpaired *t*-test. Values are mean ± SE.

controls (supplemental Fig. S3A, B, D, E). A secondary decline in photopic cone responses was also observed (Fig. 3C; supplemental Fig. S3C, F). These findings recapitulate human diseases where rods are required for cone survival and where cone loss occurs after significant rod degeneration (26). At 18 months, photoreceptor neurodegeneration was identifiable on biomicroscopy, as seen by the atrophic areas within the retina (Fig. 3D, E). These atrophic areas corresponded to hyper-reflective outer retinal foci at and above the level of the RPE on optical coherence tomography imaging (Fig. 3F). Electron microscopy demonstrated degenerative vacuolization at the junction of the RPE and the retina, confirming the biomicroscopy and optical coherence tomography findings (Fig. 3G). On histology, degenerative vacuolization of the outer retina was clearly identifiable (Fig. 3H, I). The RPE also showed structural disruption including accumulation of lipid globules, undigested photoreceptor disk fragments, and vacuoles (Fig. 3J).

Deletion of *Abca1 and Abcg1* in cone photoreceptors does not cause neurodegeneration

In addition to *Abca1/g1*$^{-rod/-rod}$ mice, we also generated *Abca1/g1*$^{-cone/-cone}$ mice to reveal the function of ABCA1 and ABCG1 in cone photoreceptors and analyzed them up to 18 months. The deletion of both *Abca1* and *Abcg1* in *Abca1/g1*$^{-cone/-cone}$ mouse cone photoreceptors was confirmed by qPCR (supplemental Fig. S4). Similar to the phenotype seen in young *Abca1/g1*$^{-rod/-rod}$ mouse retinas, young *Abca1/g1*$^{-cone/-cone}$ mouse retinas did not show any neurodegenerative phenotype at 3 months old of age (**Fig. 4A–**C). However, in distinct contrast to old *Abca1/g1*$^{-rod/-rod}$ mouse retinas, *Abca1/g1*$^{-cone/-cone}$ mouse retinas were functionally (Fig. 4D–) and histopathologically (Fig. 4J–L) normal even at 18 months of age.

ABCA1 and ABCG1 play vital roles in maintaining retinal function during metabolic stress

In order to test whether this neurodegenerative phenotype was directly related to cholesterol uptake from the blood stream and associated metabolic stress, we placed *Abca1/g1*$^{-rod/-rod}$ mice on a HFD. *Abca1/g1*$^{-rod/-rod}$ mice placed on a HFD showed significant neurodegeneration and vision loss at 3 months compared with littermate controls on a HFD (**Fig. 5A–**C). Electron microscopy demonstrated rod outer segment degeneration (Fig. 5D), accumulation of lipid globules, and undigested photoreceptor disk fragments in the RPE (Fig. 5E) in *Abca1/g1*$^{-rod/-rod}$

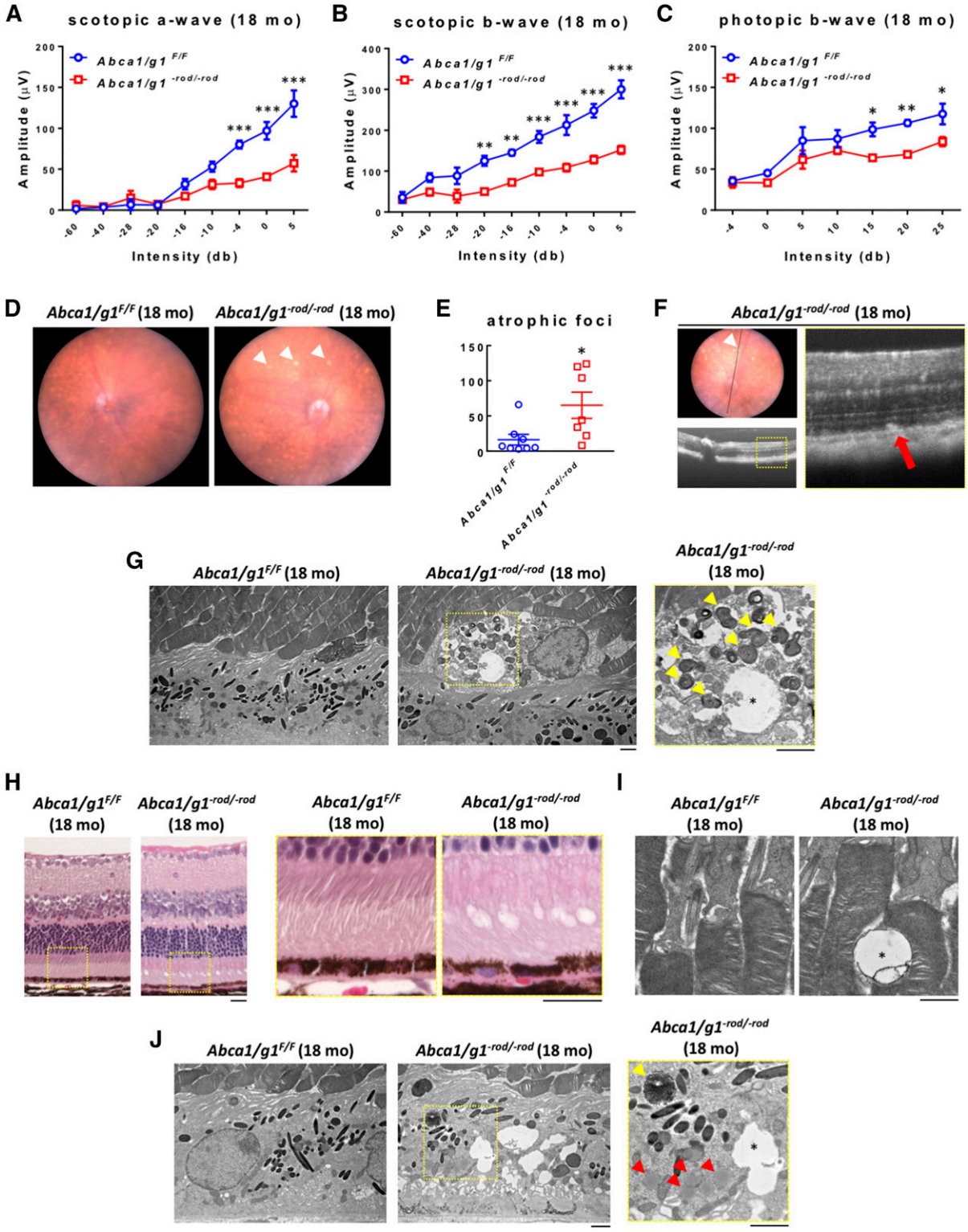

Fig. 3. *Abca1/g1*$^{-rod/-rod}$ mouse retinas (aged 18 months) show decreased scotopic and photopic responses and atrophic retinal neurodegeneration. A–C: ERG of 18-month-old *Abca1/g1*$^{F/F}$ and *Abca1/g1*$^{-rod/-rod}$ mice. *Abca1/g1*$^{F/F}$ (blue circles), n = 4; *Abca1/g1*$^{-rod/-rod}$ (red squares), n = 4. A: Scotopic a-wave amplitude. B: Scotopic b-wave amplitude. C: Photopic b-wave amplitude. $^{*}P < 0.05$, $^{**}P < 0.01$, and $^{***}P < 0.001$ by two-way ANOVA with post hoc Bonferroni's multiple comparison test. D: Representative fundus images of 18-month-old *Abca1/g1*$^{F/F}$ and *Abca1/g1*$^{-rod/-rod}$ mouse retinas. Note the atrophic appearance of *Abca1/g1*$^{-rod/-rod}$ mouse retinas (white arrowhead). E: Quantification of retinal atrophic foci per field. *Abca1/g1*$^{F/F}$ (blue circles), n = 8; *Abca1/g1*$^{-rod/-rod}$ (red squares), n = 7. $^{*}P < 0.05$ by two-tailed unpaired *t*-test. F: Representative optical coherence tomography images of 18-month-old *Abca1/g1*$^{-rod/-rod}$ mouse retinas. Note the subretinal hyper-reflective foci in *Abca1/g1*$^{-rod/-rod}$ mouse retinas (white arrowhead) corresponding to fundus atrophic appearance. G: Representative electron microscopy images of retinal atrophic foci in 18-month-old *Abca1/g1*$^{-rod/-rod}$ mouse retinas. Note the vacuoles (asterisk) and photoreceptor disk fragments (yellow arrowheads). Scale bar: 2 μm. H: Representative H&E staining images of 18-month-old *Abca1/g1*$^{F/F}$ and *Abca1/g1*$^{-rod/-rod}$

mice on a HFD, which is similar to the findings seen at 12–18 months of age in *Abca1/g1*$^{-rod/-rod}$ mice placed on a normal diet.

DISCUSSION

In this study, we hypothesized that maintaining physiologic cholesterol homeostasis in photoreceptors by ABCA1 and ABCG1 would play a key role in retinal function. In support of this hypothesis, we demonstrated that deletion of both *Abca1* and *Abcg1* in rod photoreceptors leads to age-related accumulation of cholesterol metabolites in the outer retina and retinal neurodegeneration. In addition, metabolic stress induced by a HFD significantly accelerated this neurodegenerative phenotype.

We generated *Abca1/g1*$^{-rod/-rod}$ mice to reveal the function of ABCA1 and ABCG1 in rod photoreceptors. As expected, total cholesterol levels were significantly increased in *Abca1/g1*$^{-rod/-rod}$ mouse retinas, whereas systemic lipoprotein levels were not changed. However, young *Abca1/g1*$^{-rod/-rod}$ retinas were functionally and histopathologically normal, suggesting that increased cholesterol levels in rod photoreceptors did not have acute effects on retinal structure and function. We were interested in examining the effects of aging on the retinal phenotype, as a number of neurodegenerative disease phenotypes, such as in AMD, occur with aging. As such, we aged *Abca1/g1*$^{-rod/-rod}$ mice and their littermate controls to 18 months of age and were able to demonstrate rod and subsequent cone photoreceptor degeneration and vision loss. In addition, we demonstrated that lipid droplets accumulated in the RPE of eyes from *Abca1/g1*$^{-rod/-rod}$ mice, but not in neurosensory retina, a finding consistent with the fact that one of the major functions of the RPE is phagocytosis of lipid-rich photoreceptor outer segments shed in a circadian manner. In addition, we examined the RPE complex for free cholesterol and cholesterol metabolites by LC-MS. The results confirmed increased levels of free cholesterol and several cholesterol metabolites in the RPE complex, without an increase in any of the CEs analyzed. These findings are in contrast to retinas from mice deficient in cytochrome P450 (CYP) enzymes, which showed an increase mainly in esterified cholesterols (27).

The majority of photoreceptors in murine retinas are rods, with only about 3% being cones. The ratio of rod and cone photoreceptors in human retinas is also very similar, but the distribution is different. Although aged *Abca1/g1*$^{-rod/-rod}$ mice showed significant retinal neurodegeneration, *Abca1/g1*$^{-cone/-cone}$ mouse retinas did not show any neurodegenerative phenotype, even at 18 months. These data suggest that either deletion of *Abca1* and *Abcg1* in a small percentage of photoreceptors does not impact visual function or that ABCA1 and ABCG1 are not important for normal cone function.

Finally, we tested to determine whether increased cholesterol uptake from the blood stream could affect the neurodegenerative phenotype of *Abca1/g1*$^{-rod/-rod}$ mouse retinas. In fact, cellular and tissue cholesterol level is regulated by a complex interplay between uptake and de novo biosynthesis of cholesterol, both responsible for cholesterol input and enzymatic elimination and efflux of cholesterol, which are responsible for cholesterol output. Remarkably, although short-term HFD feeding usually does not cause any retinal dysfunction in mice (21), even short-term HFD feeding to young *Abca1/g1*$^{-rod/-rod}$ mice accelerated photoreceptor neurodegeneration and vision loss, recapitulating the phenotype of aged *Abca1/g1*$^{-rod/-rod}$ mice on a normal diet. These results indicate that ABCA1 and ABCG1 play vital roles in maintaining cholesterol homeostasis in rod photoreceptors and retinal function during metabolic stress. Even in human studies, it is still controversial whether high serum cholesterol causes retinal neurodegeneration or cholesterol-lowering drugs prevent disease progression. For example, although the hallmark feature of AMD is accumulation of lipid-rich deposits underneath the RPE (called drusen), most previous studies failed to demonstrate the efficacy of cholesterol-lowering drugs, such as statins, to prevent disease progression (28, 29). Our study clearly revealed that, in the limited condition of disrupted cholesterol metabolism in rod photoreceptors, HFD caused retinal neurodegeneration. This fact might give us a new insight into the relationship between HFD or serum cholesterol and retinal neurodegenerative diseases such as AMD.

In summary, this study identifies cholesterol homeostasis as a critical regulator of age-related rod photoreceptor neurodegeneration and provides a unifying metabolic mechanism of vision loss in diverse retinal degenerative diseases. Accumulation of cholesterol and its metabolites in the outer retina may be a danger signal that leads to chronic lipotoxicity and neurodegeneration. These findings have potential translational relevance, as multiple genome-wide association studies have identified polymorphisms in genes involved in cholesterol metabolism, in general, and ABC transporters, in particular, in diseases such as AMD (30, 31) and Stargardts disease (32, 33) that are characterized by lipoprotein deposition and retinal neurodegeneration. In addition, these findings have potential implications beyond the eye, as recent studies also demonstrate a role for cholesterol clearance in regulating myelination of the CNS (34). Targeted metabolic interventions that regulate ABCA1 and ABCG1 in the retina may thus provide potential therapeutic avenues and prevent vision loss.

mouse retinas. Note the degenerative vacuolization of the outer retina. Scale bar: 20 μm. I, J: Representative electron microscopy images of 18-month-old *Abca1/g1*$^{F/F}$ and *Abca1/g1*$^{-rod/-rod}$ mouse retinas. I: Vacuoles in outer segment of *Abca1/g1*$^{-rod/-rod}$ mouse retinas (asterisk). Scale bar: 1 μm. J: Accumulation of lipid globules (red arrowheads), undigested photoreceptor disk fragments (yellow arrowhead), and vacuoles (asterisk) within the RPE. Scale bar: 2 μm. Values are mean ± SE.

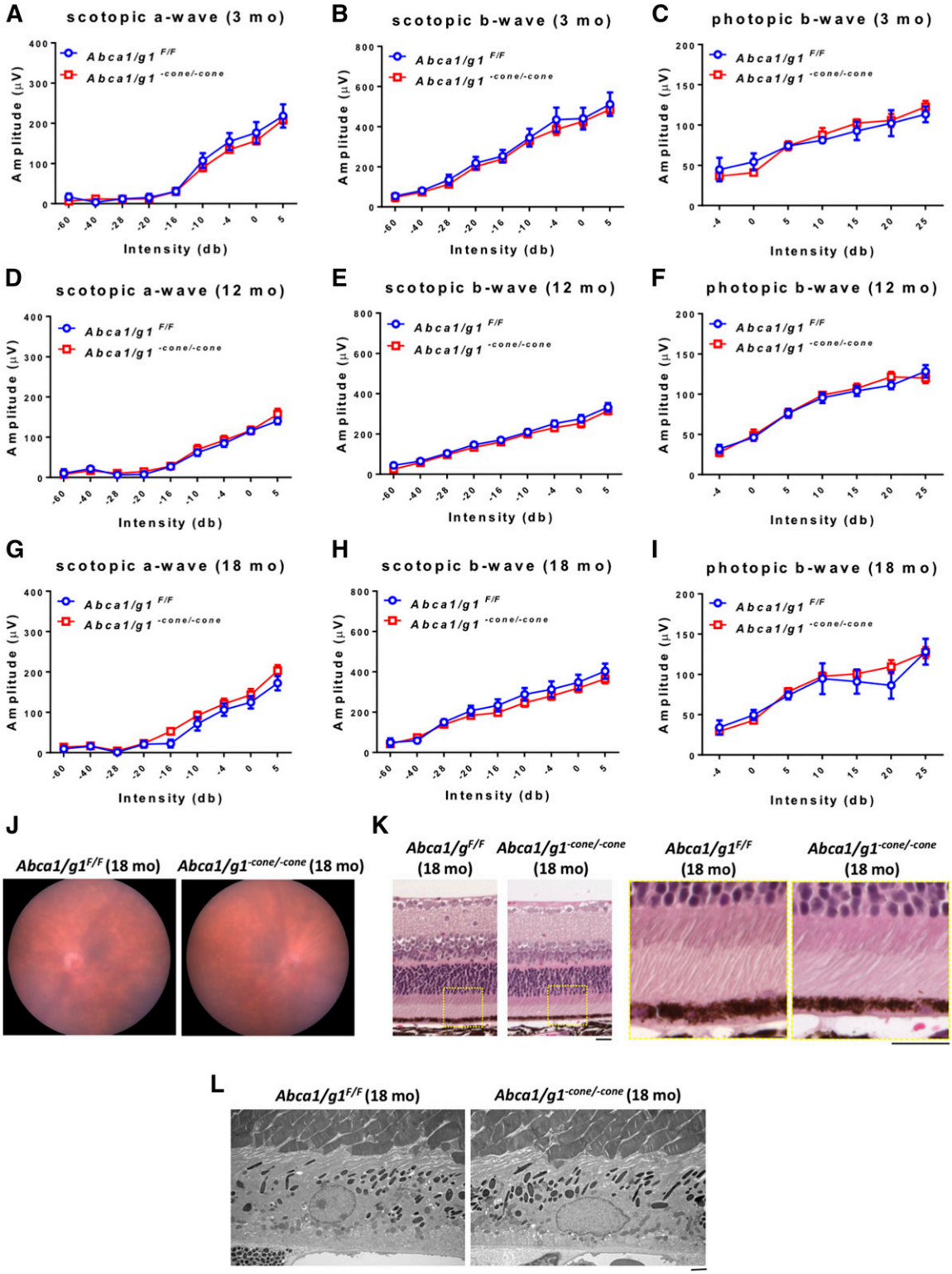

Fig. 4. Deletion of *Abca1* and *Abcg1* in cone photoreceptors does not cause detectable neurodegeneration. A–C: ERG of 3-month-old *Abca1/g1*$^{F/F}$ and *Abca1/g1*$^{-cone/-cone}$ mice. *Abca1/g1*$^{F/F}$ (blue circles), n = 5; *Abca1/g1*$^{-cone/-cone}$ (red squares), n = 6. A: Scotopic a-wave amplitude. B: Scotopic b-wave amplitude. C: Photopic b-wave amplitude. D–F: ERG of 12-month-old *Abca1/g1*$^{F/F}$ and *Abca1/g1*$^{-cone/-cone}$ mice. *Abca1/g1*$^{F/F}$ (blue circles), n = 7; *Abca1/g1*$^{-cone/-cone}$ (red squares), n = 7. D: Scotopic a-wave amplitude. E: Scotopic b-wave amplitude. F: Photopic b-wave amplitude. No significant difference was detected by two-way ANOVA. G–I: ERG of 18-month-old *Abca1/g1*$^{F/F}$ and *Abca1/g1*$^{-cone/-cone}$ mice. *Abca1/g1*$^{F/F}$ (blue circles), n = 4; *Abca1/g1*$^{-cone/-cone}$ (red squares), n = 6. G: Scotopic a-wave amplitude. H: Scotopic b-wave amplitude. I: Photopic b-wave amplitude. No significant difference was detected by two-way ANOVA. J: Representative fundus images of 18-month-old *Abca1/g1*$^{F/F}$ and *Abca1/g1*$^{-cone/-cone}$ mouse retinas. K: Representative H&E staining images of 18-month-old *Abca1/g1*$^{F/F}$ and *Abca1/g1*$^{-cone/-cone}$ mouse retinas. Scale bars: 20 μm. L: Representative electron microscopy images of 18-month-old *Abca1/g1*$^{F/F}$ and *Abca1/g1*$^{-cone/-cone}$ mouse retinas. Scale bars: 2 μm. Values are mean ± SE.

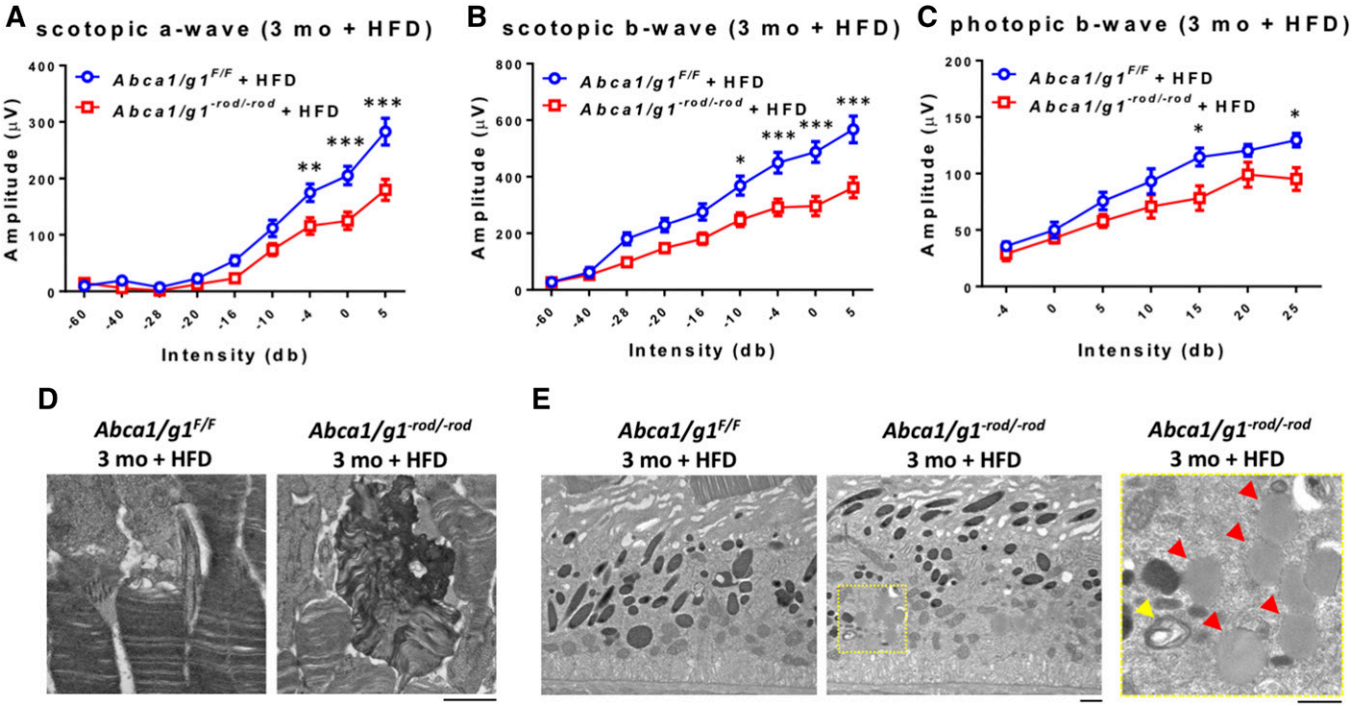

Fig. 5. A HFD significantly accelerates retinal neurodegeneration in *Abca1/g1*$^{-rod/-rod}$ mice. A–C: ERG of 3-month-old *Abca1/g1*$^{F/F}$ and *Abca1/g1*$^{-rod/-rod}$ mice on a HFD. *Abca1/g1*$^{F/F}$ on a HFD (blue circles), n = 6; *Abca1/g1*$^{-rod/-rod}$ on a HFD (red squares), n = 9. A: Scotopic a-wave amplitude. B: Scotopic b-wave amplitude. C: Photopic b-wave amplitude. *P < 0.05, **P < 0.01, and ***P < 0.001 by two-way ANOVA with post hoc Bonferroni's multiple comparison test. D, E: Representative electron microscopy images of 3-month-old *Abca1/g1*$^{F/F}$ and *Abca1/g1*$^{-rod/-rod}$ mouse retinas on a HFD. D: Dysmorphic changes within outer segments of *Abca1/g1*$^{-rod/-rod}$ mouse retinas on a HFD. Scale bar: 1 μm. E: Accumulation of lipid globules (red arrowheads) and undigested photoreceptor disk fragments (yellow arrowhead) in the RPE. Scale bars: 1 μm. Values are mean ± SE.

The authors thank Wandy L. Beatty for electron microscopy analyses.

REFERENCES

1. Arenas, F., C. Garcia-Ruiz, and J. C. Fernandez-Checa. 2017. Intracellular cholesterol trafficking and impact in neurodegeneration. *Front. Mol. Neurosci.* **10:** 382.
2. Fliesler, S. J., and L. Bretillon. 2010. The ins and outs of cholesterol in the vertebrate retina. *J. Lipid Res.* **51:** 3399–3413.
3. Athanasiou, D., M. Aguila, J. Bellingham, W. Li, C. McCulley, P. J. Reeves, and M. E. Cheetham. 2018. The molecular and cellular basis of rhodopsin retinitis pigmentosa reveals potential strategies for therapy. *Prog. Retin. Eye Res.* **62:** 1–23.
4. Bowes Rickman, C., S. Farsiu, C. A. Toth, and M. Klingeborn. 2013. Dry age-related macular degeneration: mechanisms, therapeutic targets, and imaging. *Invest. Ophthalmol. Vis. Sci.* **54:** ORSF68–ORSF80.
5. Niven, J. E., and S. B. Laughlin. 2008. Energy limitation as a selective pressure on the evolution of sensory systems. *J. Exp. Biol.* **211:** 1792–1804.
6. Okawa, H., A. P. Sampath, S. B. Laughlin, and G. L. Fain. 2008. ATP consumption by mammalian rod photoreceptors in darkness and in light. *Curr. Biol.* **18:** 1917–1921.
7. Goldberg, A. F., O. L. Moritz, and D. S. Williams. 2016. Molecular basis for photoreceptor outer segment architecture. *Prog. Retin. Eye Res.* **55:** 52–81.
8. Albert, A., D. Alexander, and K. Boesze-Battaglia. 2016. Cholesterol in the rod outer segment: a complex role in a "simple" system. *Chem. Phys. Lipids.* **199:** 94–105.
9. Storti, F., G. Raphael, V. Griesser, K. Klee, F. Drawnel, C. Willburger, R. Scholz, T. Langmann, A. von Eckardstein, J. Fingerle, et al. 2017. Regulated efflux of photoreceptor outer segment-derived cholesterol by human RPE cells. *Exp. Eye Res.* **165:** 65–77.
10. Sene, A., and R. S. Apte. 2014. Eyeballing cholesterol efflux and macrophage function in disease pathogenesis. *Trends Endocrinol. Metab.* **25:** 107–114.
11. Sene, A., A. A. Khan, D. Cox, R. E. Nakamura, A. Santeford, B. M. Kim, R. Sidhu, M. D. Onken, J. W. Harbour, S. Hagbi-Levi, et al. 2013. Impaired cholesterol efflux in senescent macrophages promotes age-related macular degeneration. *Cell Metab.* **17:** 549–561.
12. Duncan, K. G., K. Hosseini, K. R. Bailey, H. Yang, R. J. Lowe, M. T. Matthes, J. P. Kane, M. M. LaVail, D. M. Schwartz, and J. L. Duncan. 2009. Expression of reverse cholesterol transport proteins ATP-binding cassette A1 (ABCA1) and scavenger receptor BI (SR-BI) in the retina and retinal pigment epithelium. *Br. J. Ophthalmol.* **93:** 1116–1120.
13. Ananth, S., J. P. Gnana-Prakasam, Y. D. Bhutia, R. Veeranan-Karmegam, P. M. Martin, S. B. Smith, and V. Ganapathy. 2014. Regulation of the cholesterol efflux transporters ABCA1 and ABCG1 in retina in hemochromatosis and by the endogenous siderophore 2,5-dihydroxybenzoic acid. *Biochim. Biophys. Acta.* **1842:** 603–612.
14. Li, S., D. Chen, Y. Sauve, J. McCandless, Y. J. Chen, and C. K. Chen. 2005. Rhodopsin-iCre transgenic mouse line for Cre-mediated rod-specific gene targeting. *Genesis.* **41:** 73–80.
15. Lin, J. B., S. Kubota, N. Ban, M. Yoshida, A. Santeford, A. Sene, R. Nakamura, N. Zapata, M. Kubota, K. Tsubota, et al. 2016. NAMPT-mediated NAD(+) biosynthesis is essential for vision in mice. *Cell Reports.* **17:** 69–85.
16. Le, Y. Z., J. D. Ash, M. R. Al-Ubaidi, Y. Chen, J. X. Ma, and R. E. Anderson. 2004. Targeted expression of Cre recombinase to cone photoreceptors in transgenic mice. *Mol. Vis.* **10:** 1011–1018.
17. Westerterp, M., S. Gourion-Arsiquaud, A. J. Murphy, A. Shih, S. Cremers, R. L. Levine, A. R. Tall, and L. Yvan-Charvet. 2012. Regulation of hematopoietic stem and progenitor cell mobilization by cholesterol efflux pathways. *Cell Stem Cell.* **11:** 195–206.
18. Westerterp, M., A. J. Murphy, M. Wang, T. A. Pagler, Y. Vengrenyuk, M. S. Kappus, D. J. Gorman, P. R. Nagareddy, X. Zhu, S. Abramowicz, et al. 2013. Deficiency of ATP-binding cassette transporters A1 and G1 in macrophages increases inflammation and accelerates atherosclerosis in mice. *Circ. Res.* **112:** 1456–1465.
19. Zhou, Z., F. Vinberg, F. Schottler, T. A. Doggett, V. J. Kefalov, and T. A. Ferguson. 2015. Autophagy supports color vision. *Autophagy.* **11:** 1821–1832.

20. Mattapallil, M. J., E. F. Wawrousek, C. C. Chan, H. Zhao, J. Roychoudhury, T. A. Ferguson, and R. R. Caspi. 2012. The Rd8 mutation of the Crb1 gene is present in vendor lines of C57BL/6N mice and embryonic stem cells, and confounds ocular induced mutant phenotypes. *Invest. Ophthalmol. Vis. Sci.* **53:** 2921–2927.
21. Rajagopal, R., G. W. Bligard, S. Zhang, L. Yin, P. Lukasiewicz, and C. F. Semenkovich. 2016. Functional deficits precede structural lesions in mice with high-fat diet-induced diabetic retinopathy. *Diabetes.* **65:** 1072–1084.
22. Feodorova, Y., M. Koch, S. Bultman, S. Michalakis, and I. Solovei. 2015. Quick and reliable method for retina dissociation and separation of rod photoreceptor perikarya from adult mice. *MethodsX.* **2:** 39–46.
23. Skaper, S. D. 2012. Isolation and culture of rat cone photoreceptor cells. *Methods Mol. Biol.* **846:** 147–158.
24. Santeford, A., L. A. Wiley, S. Park, S. Bamba, R. Nakamura, A. Gdoura, T. A. Ferguson, P. K. Rao, J. L. Guan, T. Saitoh, et al. 2016. Impaired autophagy in macrophages promotes inflammatory eye disease. *Autophagy.* **12:** 1876–1885.
25. Ding, J. D., R. Y. Salinas, and V. Y. Arshavsky. 2015. Discs of mammalian rod photoreceptors form through the membrane evagination mechanism. *J. Cell Biol.* **211:** 495–502.
26. Aït-Ali, N., R. Fridlich, G. Millet-Puel, E. Clérin, F. Delalande, C. Jaillard, F. Blond, L. Perrocheau, S. Reichman, L. C. Byrne, et al. 2015. Rod-derived cone viability factor promotes cone survival by stimulating aerobic glycolysis. *Cell.* **161:** 817–832.
27. Saadane, A., N. Mast, T. Dao, B. Ahmad, and I. A. Pikuleva. 2016. Retinal hypercholesterolemia triggers cholesterol accumulation and esterification in photoreceptor cells. *J. Biol. Chem.* **291:** 20427–20439.
28. Maguire, M. G., G. S. Ying, C. A. McCannel, C. Liu, and Y. Dai; Complications of Age-related Macular Degeneration Prevention Trial (CAPT) Research Group. 2009. Statin use and the incidence of advanced age-related macular degeneration in the Complications of Age-related Macular Degeneration Prevention Trial. *Ophthalmology.* **116:** 2381–2385.
29. Al-Holou, S. N., W. R. Tucker, E. Agrón, T. E. Clemons, C. Cukras, F. L. Ferris III, and E. Y. Chew; Age-Related Eye Disease Study 2 Research Group. 2015. The association of statin use with age-related macular degeneration progression: the Age-Related Eye Disease Study 2 Report Number 9. *Ophthalmology.* **122:** 2490–2496.
30. Chen, W., D. Stambolian, A. O. Edwards, K. E. Branham, M. Othman, J. Jakobsdottir, N. Tosakulwong, M. A. Pericak-Vance, P. A. Campochiaro, M. L. Klein, et al. 2010. Genetic variants near TIMP3 and high-density lipoprotein-associated loci influence susceptibility to age-related macular degeneration. *Proc. Natl. Acad. Sci. USA.* **107:** 7401–7406.
31. Neale, B. M., J. Fagerness, R. Reynolds, L. Sobrin, M. Parker, S. Raychaudhuri, P. L. Tan, E. C. Oh, J. E. Merriam, E. Souied, et al. 2010. Genome-wide association study of advanced age-related macular degeneration identifies a role of the hepatic lipase gene (LIPC). *Proc. Natl. Acad. Sci. USA.* **107:** 7395–7400.
32. Allikmets, R. 1997. A photoreceptor cell-specific ATP-binding transporter gene (ABCR) is mutated in recessive Stargardt macular dystrophy. *Nat. Genet.* **17:** 122.
33. Quazi, F., and R. S. Molday. 2013. Differential phospholipid substrates and directional transport by ATP-binding cassette proteins ABCA1, ABCA7, and ABCA4 and disease-causing mutants. *J. Biol. Chem.* **288:** 34414–34426.
34. Cantuti-Castelvetri, L., D. Fitzner, M. Bosch-Queralt, M. T. Weil, M. Su, P. Sen, T. Ruhwedel, M. Mitkovski, G. Trendelenburg, D. Lutjohann, et al. 2018. Defective cholesterol clearance limits remyelination in the aged central nervous system. *Science.* **359:** 684–688.